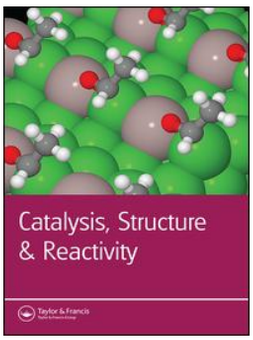

Catalysis, Structure & Reactivity

ISSN: 2055-074X (Print) 2055-0758 (Online) Journal homepage: https://www.tandfonline.com/loi/ycsr20

Effect of Cu content on the bimetallic Pt–Cu catalysts for propane dehydrogenation

Zixue Ma, Zhenwei Wu & Jeffrey T. Miller

To cite this article: Zixue Ma, Zhenwei Wu & Jeffrey T. Miller (2017) Effect of Cu content on the bimetallic Pt–Cu catalysts for propane dehydrogenation, Catalysis, Structure & Reactivity, 3:1-2, 43-53, DOI: 10.1080/2055074X.2016.1263177

To link to this article: https://doi.org/10.1080/2055074X.2016.1263177

Published online: 21 Feb 2017.

CATALYSIS, STRUCTURE & REACTIVITY, 2017
VOL. 3, NOS. 1–2, 43–53
http://dx.doi.org/10.1080/2055074X.2016.1263177

Taylor & Francis
Taylor & Francis Group

ORIGINAL RESEARCH PAPER

OPEN ACCESS

Effect of Cu content on the bimetallic Pt–Cu catalysts for propane dehydrogenation

Zixue Ma, Zhenwei Wu and Jeffrey T. Miller

Davidson School of Chemical Engineering, Purdue University, West Lafayette, IN, USA

ABSTRACT

Silica supported, 2 nm Pt and Pt–Cu catalysts with different Cu:Pt atomic ratios and similar size were evaluated for propane dehydrogenation at 550 °C. Monometallic Pt showed low propylene selectivity of 61% at 20% conversion and a TOR of 0.06 s^{-1}. For the Pt–Cu catalysts, the dehydrogenation selectivity and TOR continuously increased with increasing Cu level in the nanoparticle, to eventually 96% selective at 20% conversion with a TOR of 0.98 s^{-1} for a catalyst with a Cu:Pt atomic ratio of 7.3. Synchrotron *in situ* X-ray diffraction and X-ray absorption spectroscopy analysis showed that Pt–Cu catalysts with increasing Cu loading formed solid solution type bimetallic structures. For example, a Pt–Cu catalyst with Cu:Pt atomic ratio of 7.3 formed solid solution containing 87% Cu. In this catalyst, the Pt active sites were geometrically isolated by the inactive metallic Cu, which was suggested to be responsible for high selectivity to propane dehydrogenation. The Cu neighbors surrounding the Pt also likely modified the energy level of Pt 5d orbitals and contribute to a TOR about 16 times higher than that of monometallic Pt.

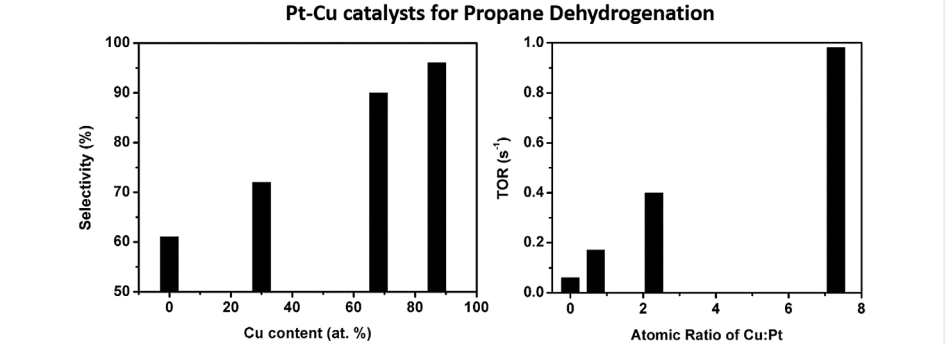

ARTICLE HISTORY
Received 29 September 2016
Accepted 15 November 2016

KEYWORDS
Light alkane dehydrogenation; bimetallic nanoparticle catalyst; solid solution; *in situ* synchrotron X-ray diffraction; *in situ* X-ray absorption spectroscopy

Introduction

For the conversion of the abundant shale gas resources, Pt bimetallic catalysts are used in light olefin production through alkane dehydrogenation. Compared to other group VIII metals, platinum is preferably used for light alkane dehydrogenation catalyst because of its relatively high selectivity favoring paraffinic C–H bond activation over C–C bond activation [1]. To obtain optimal performance, a promoter is added to modify the properties of platinum catalysts, for example, Sn, Zn, In and Ga are highly selective for propane dehydrogenation and Pt-Sn catalyst is used commercially [2–10]. The promoters have been reported to suppress side reactions, e.g. hydrogenolysis, coking and metal sintering [4,6,11].

Recently, it was reported that certain intermetallic alloy catalysts containing Pd-Zn and Pd-In are also highly selective to light alkane dehydrogenation [12–14]. Monometallic Pd catalysts had poor olefin selectivity, typically below about 50%. After addition of Zn or In to Pd, the olefin selectivity increased to near 100%. This high dehydrogenation selectivity was proposed to originate from the formation of the PdZn and PdIn intermetallic alloy structure on the catalyst surface which geometrically isolated the Pd catalytic sites by non-catalytic Zn or In atoms [12,13], i.e. a site isolation effect. This geometric effect is very likely also applicable to other active metals including Pt and other promoters.

Cu can form bimetallic nanoparticles with Pt [15]. Previously, addition of copper has been reported to

CONTACT Jeffrey T. Miller mill1194@purdue.edu

promote Pt light alkane dehydrogenation catalysts [16–19]. It was suggested that addition of Cu increased the dehydrogenation selectivity of the catalysts from 77.2 to 90.8% [18], although at the expense of decreasing the catalyst dispersion due to surface coverage by Cu [16,17]. An electronic interaction between Pt and Cu was proposed lead to suppressed propylene adsorption and increased energy barrier for C–C bond rupture, which also reduced coke formation [18]. The specific structure of the Pt–Cu catalysts, however, hasn't been investigated in detail. For the Pt–Cu binary system, both intermetallic alloys and solid solutions are possible [17,19]. The transformation temperature for Pt–Cu alloys from ordered intermetallics to disordered solid solution is around 600–800 °C for bulk materials [15] but may be lower for nanoparticles, therefore, close to the dehydrogenation reaction temperature. *In situ* structural characterization on relevant nanoparticles is needed for understanding the Pt–Cu catalysts structure and rational control of the Cu promotion for Pt–Cu catalysts.

To explore the structure of Pt–Cu catalysts and its relation to the catalytic performance, we report the synthesis, characterization and testing of Pt and three Pt–Cu catalysts supported on silica with different Cu:Pt atomic ratios. The catalysts were characterized by atomic absorption spectroscopy, CO chemisorption, scanning transmission electron microscopy (STEM), *in situ* synchrotron X-ray absorption spectroscopy (XAS) and *in situ* synchrotron X-ray diffraction (*in situ* XRD). Propane dehydrogenation was used to evaluate the effect of Cu on the catalytic performance of the catalysts.

Experimental methods

Catalyst synthesis

A monometallic Pt catalyst with 3 wt.% of Pt on silica was synthesized by incipient wetness impregnation method. 0.297 g of tetraamine platinum nitrate $(NH_3)_4Pt(NO_3)_2$ (Sigma–Aldrich) was dissolved in 4 ml of de-ionized water. Ammonia was added to the solution until the pH was greater than 10. This solution was then added drop-wise to 5 g of silica (Davisil 636 silica gel from Sigma–Aldrich) and mixed. The catalyst was dried overnight at 125 °C, calcined at 250 °C for 3 h and then reduced at 550 °C in H_2 for 30 min.

Three silica supported Pt–Cu catalysts with different Pt and Cu loading (see Table 1) were synthesized by co-incipient wetness impregnation (co-IWI) method using tetraamine platinum nitrate $(NH_3)_4Pt(NO_3)_2$ (Sigma–Aldrich) and copper nitrate trihydrate $Cu(NO_3)_2{\cdot}3H_2O$ (Sigma–Aldrich). For the Cu–Pt(0.7) catalyst, 0.094 g of $Cu(NO_3)_2{\cdot}3H_2O$ was dissolved in 1 ml of de-ionized water and ammonia was added until the pH was greater than 10. Then, 0.198 g of $(NH_3)_4Pt(NO_3)_2$ was added to the solution and de-ionized water was added to bring the total volume to 4 ml. The obtained solution was added drop-wise to 5 g of SiO_2 and stirred. After drying at 125 °C overnight, the solids were calcined at 250 °C in air for 3 h. The catalyst was reduced by flowing H_2 at 550 °C for 30 min. After reduction, nitrogen was purged again and the catalyst was cooled to room temperature. The other catalysts (see Table 1) with different Pt and Cu loading were prepared in the same procedure except that different amount of Pt and Cu salts was used.

Atomic absorption spectroscopy

The elemental loadings of Pt and Cu in the catalyst samples were measured using a PerkinElmer Analyst 300 atomic absorption spectrometer. Approximately 50 mg of the Pt–Cu catalysts were ground and dissolved in 10 ml aqua regia overnight followed by the addition of about 30 ml D.I. water to dilute the concentrated acid solution. Atomic absorption spectroscopy (AAS) standards for Pt and Cu (Fluka) were used for calibrating the instrument. Weight percentages of Pt and Cu were calculated from the absorbance value.

Scanning transmission electron microscopy

The STEM images were obtained at Birck Nanotechnology Center at Purdue University using the FEI Titan Scanning Transmission Electron Microscope (80–300 kV, 1 nm spatial resolution in STEM). Catalysts samples were dispersed in isopropyl alcohol. Three drops of the solution were added to an ultrathin Carbon film-Au TEM ready grid (TedPella) and dried on a hot plate at 80 °C. Images were taken using the high angle annular dark field (HAADF) detector at 300 kV. A minimum of 100 particles were counted to determine the size distribution for each sample by using the ImageJ program [20].

CO chemisorption

The CO chemisorption measurements on Pt–Cu catalysts were conducted using a Micromeritics ASAP 2020 chemisorption instrument. Catalysts (around 0.1 g) were

Table 1. Elemental analysis, particle sizes and catalyst dispersion.

Sample name [a]	Weight loading of Pt (wt.%)	Weight loading of Cu (wt.%)	Atomic ratio of Cu:Pt	STEM particle size (nm)	Dispersion (%)
Pt	3.0	/	/	2.5 ± 0.4	29
Cu–Pt(0.7)	1.8	0.5	0.7	2.5 ± 0.4	18
Cu–Pt(2.3)	2.0	1.5	2.3	2.2 ± 0.4	17
Cu–Pt(7.3)	0.7	1.6	7.3	2.1 ± 0.4	24

[a]The numbers in the parenthesis refer to the atomic ratio of Cu to Pt of the Pt–Cu catalysts, Pt refers to the monometallic Pt catalyst.

loaded into a U-shaped quartz reactor tube. The catalysts were reduced in H_2/He at 550 °C for 30 min and then flushed for 30 min in He before evacuation and measurements. The catalyst dispersion was determined from the difference analysis of the chemisorption curve. A stoichiometry of CO: Pt = 1:1 was assumed to estimate the dispersion value for Pt–Cu catalysts.

Propane dehydrogenation

Propane dehydrogenation performance was tested on the Pt and Pt–Cu catalysts diluted with silica. The weight of catalysts used for the measurement ranged from 40 to 100 mg. The diluted catalyst mixture was loaded into a quartz fixed-bed reactor with 3/8-inch ID. The catalysts were reduced in 50 cm^3/min of 5 % H_2/N_2 as the temperature increased to the reaction temperature at 550 °C for 30 min. The reactor was then purged with N_2 for 5 min before the pre-mixed reactant feed gas consisting of 100 ccm 5% propane/N_2 and 100 ccm 5% hydrogen/N_2 was flowed to the reactor. The tests were run until the conversion and selectivity reached steady state or the conversion is very low. To determine how propane dehydrogenation selectivity varies with conversion for the fresh Pt and Pt–Cu catalysts, the reaction tests were conducted over a range of conversion from around 10–30% by changing the weight of the catalysts and the total flow rate of the reactant mixture. The initial conversion and selectivity value at $t = 0$ were then obtained from extrapolation of the measured conversion and selectivity vs. time on stream using an exponential fit. These selectivity values were plot against conversion to show the behavior of Pt and Pt–Cu catalysts.

In situ X-ray absorption spectroscopy

X-ray absorption spectroscopy measurements at the Pt L_{III} edge (11.564 keV) and Cu K edge (8.979 keV) were performed at the 10-BM on the bending magnet beamline of the Materials Research Collaborative Access Team (MRCAT) at the Advanced Photon Source (APS), Argonne National Laboratory. Samples were ground into a fine powder and pressed into a sample holder. The loaded sample holder was then placed in a quartz tube. The samples were reduced at 550 °C in a 3% H_2/He mixture at 100 cm^3/min flow rate. After reduction, the samples were purged with He at 100 cm^3/min flow rate and cooled to room temperature before the spectra were recorded *in situ*.

WinXAS software was used to fit the XAS data [21]. The EXAFS coordination parameters were obtained by a least squares fit in *R*-space of the k^2-weighted Fourier transform data from $\Delta k = 3.0$ to 12.0 $Å^{-1}$. The first shell fit of the magnitude and imaginary parts were performed between $\Delta R = 1.6$ to 2.8 Å for both the Pt and Cu edge. The samples were independently fit to get the best coordination number (CN) and σ^2 values for each sample. These were each similar, though not exact. Since σ^2 is correlated with the coordination number, in order to compare small changes in CN a consistent value is used for σ^2. Thus, σ^2 is fixed as the average value of all fits for the individual samples. This is reasonable since these catalysts have similar size and the same type of scatterings (each scattering pair should have the same σ^2). Fixing the σ^2 of the same type of scattering to be the same allows for systematic comparison of the CN values between different samples. Finally, model fits were also performed with σ^2 values 0.001–0.002 higher and lower than the chosen ones and the obtained CN values were within the errors of EXAFS, i.e. ca. 5% compared to the result shown in Table 3. The fits did not initially impose the constraints that the bond distance of Pt–Cu must equal Cu–Pt, yet the best fit values resulted in this relation. Once this relation was verified, we fixed the Pt–Cu and Cu–Pt at the same and most consistent value for all samples. The CNs were also initially fit with no constraints. However, the obtained CNs were actually very close to the required relationship $CN_{ab} \times MF_a = CN_{ba} \times MF_b$ (MF is mole fraction) for bimetallic particles. By not forcing this correlation in the fit, this gives confidence that the CN and σ^2 values are close to the correct values.

In situ, synchrotron XRD

In situ XRD measurements the Pt and Pt–Cu catalysts were performed at the 11-ID-C beamline at the APS, Argonne National Laboratory. Data was collected in transmission mode using X-rays with energy of 105.59 keV ($\lambda = 0.117418$ Å) and a PerkinElmer large area detector with typical exposure times of 5 s and a total of 30 scans. Samples were loaded into a Linkam Thermal Stage allowing reactant gas flow. The loaded catalyst was reduced in 3% H_2/He with a flow rate of 100 cm^3/min at 550 °C when a measurement was conducted. The stage was then cooled to room temperature for another measurement to be taken. The SiO_2 support and the empty cell were treated to the same procedure and reference measurements taken at the same condition for background subtraction. The 2-D diffraction patterns were integrated to 1-D scattering intensity vs. 2θ data by GSASII software [22]. Materials Analysis Using Diffraction software was used to generate the diffraction pattern of potential phases under the measurement condition to help determine the crystal phase of each sample [23].

Results

Particle size and catalyst dispersion

A monometallic Pt and three Pt–Cu catalysts with different Cu:Pt atomic ratio as confirmed by atomic absorption spectra results (Table 1) were studied. Their particle sizes were determined by STEM imaging. Images were taken for all four catalysts after pre-reduction in H_2 at

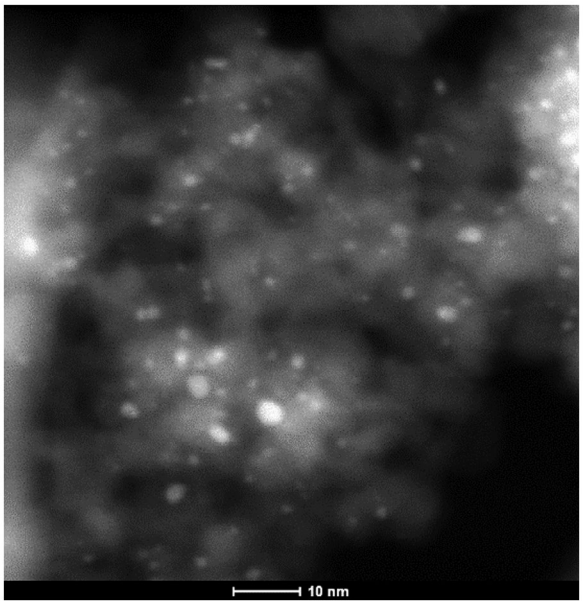

Figure 1. STEM HAADF image of Cu–Pt(2.3) catalyst.

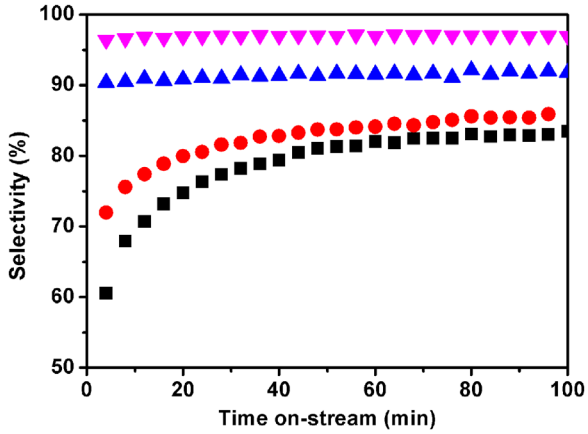

Figure 2. Propylene selectivity vs. time measured at 550 °C for the Pt (black squares), Cu–Pt(0.7) (red circles), Cu–Pt(2.3) (blue triangles), and Cu–Pt(7.3) (magenta down triangles) catalysts.

550 °C and exposure to air. An image of Cu–Pt(2.3) catalyst is shown in Figure 1 and are typical of the other samples. The average particle size of this sample was determined to be 2.2 nm with a standard deviation of 0.4 nm. Obtained average particle sizes for the other samples are reported in Table 1. All the catalysts have similar particle size between 2 and 3 nm. The similar particle sizes of these catalysts enable comparison between their kinetics and surface structure without having to account for the changes in particle size.

The Pt dispersions of the catalysts were determined from CO chemisorption with a stoichiometry of CO: Pt = 1: 1. The dispersion for monometallic Pt was found to be 29%, slightly lower than the value expected from the particle size. For Pt–Cu catalysts with similar particle size, the dispersions were all lower than the monometallic catalysts. They were found to be 18% for Cu–Pt(0.7) and 17% for Cu–Pt(2.3) catalysts, suggesting potential surface coverage by Cu atoms. The dispersion of the Cu–Pt(7.3) catalyst was 24%, slightly larger than the other Pt–Cu catalysts.

Table 2. Propane dehydrogenation performance of the Pt and Pt–Cu catalysts.

Catalyst	Propylene selectivity at 20% conversion (%)	Rate per gram Pt (mol g^{-1} s^{-1})	TOR (s^{-1})
Pt	61	8.8×10^{-5}	0.06
Cu–Pt(0.7)	72	1.6×10^{-4}	0.17
Cu–Pt(2.3)	90	3.5×10^{-4}	0.40
Cu–Pt(7.3)	96	1.2×10^{-3}	0.98

Propane dehydrogenation

The Pt and Pt–Cu catalysts were evaluated for propane dehydrogenation in the presence of H_2 and at 550 °C. The catalyst selectivity vs. time on stream were measured at an initial conversion of about 20% (Figure 2). All the catalysts deactivated with time on stream due to side reaction hydrogenolysis and coking and the conversion dropped to 12–13% after 1 h. The selectivity increased or maintained with time on stream as the catalyst deactivated and likely the surface sites catalyzing hydrogenolysis reactions are gradually covered by the coke. The Pt catalyst started with a propylene selectivity of 61% (Table 2). After 1 h at 12% conversion, the selectivity increased to about 82% when the catalyst performance started to stabilize. The Cu–Pt(0.7) catalyst with relatively low amount of Cu showed a better initial selectivity of 72%. The catalyst went through deactivation similar to that of Pt and reached a slightly higher stable selectivity around 85% after 1 h. For Cu–Pt(2.3) and Cu–Pt(7.3) catalysts, however, their initial dehydrogenation selectivity was greatly improved to 90% for the former and 96% for the latter. Both catalysts maintained their high selectivity throughout the test, without major change in selectivity with time.

To further investigate the different catalyst performance, the propylene selectivity of Cu–Pt(7.3) at different conversions (Figure 3(a)) was compared with the monometallic Pt. For the latter, there was a large change in selectivity from 72 to 52% with changing conversion from 10 to 30%, while the selectivity of Pt–Cu remained high selectivity at over 95% to propylene.

Significant differences in the reaction rate are also observed for Pt and Pt–Cu. Monometallic Pt catalyzed propane dehydrogenation at 550 °C with a rate of 8.8×10^{-5} mol g^{-1} s^{-1}. For Cu–Pt(0.7) catalysts, however, the rate per gram Pt was 1.6×10^{-4} mol g^{-1} s^{-1}, almost doubled from Pt. When more Cu was introduced into the catalysts, for Cu–Pt(2.3) catalyst, the catalytic rate per gram Pt further increased by more than 2 times compared to Cu–Pt(0.7). Higher amounts of Cu resulted in even higher rate as observed for Cu–Pt(7.3) catalyst. Normalizing the rate to the number of surface Pt atoms

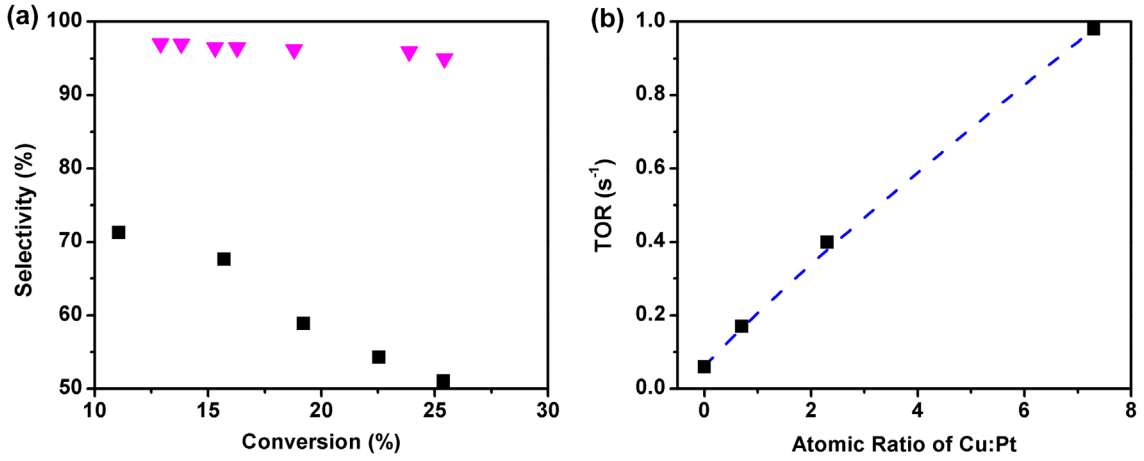

Figure 3. (a) Propylene selectivity vs. propane conversion measured at 550 °C for the Pt (black squares), and Cu–Pt(7.3) (magenta down triangles) catalysts. (b) TOR vs. atomic ratio of Cu:Pt for Pt, Cu–Pt(0.7), Cu–Pt(2.3), and Cu–Pt(7.3) catalysts.

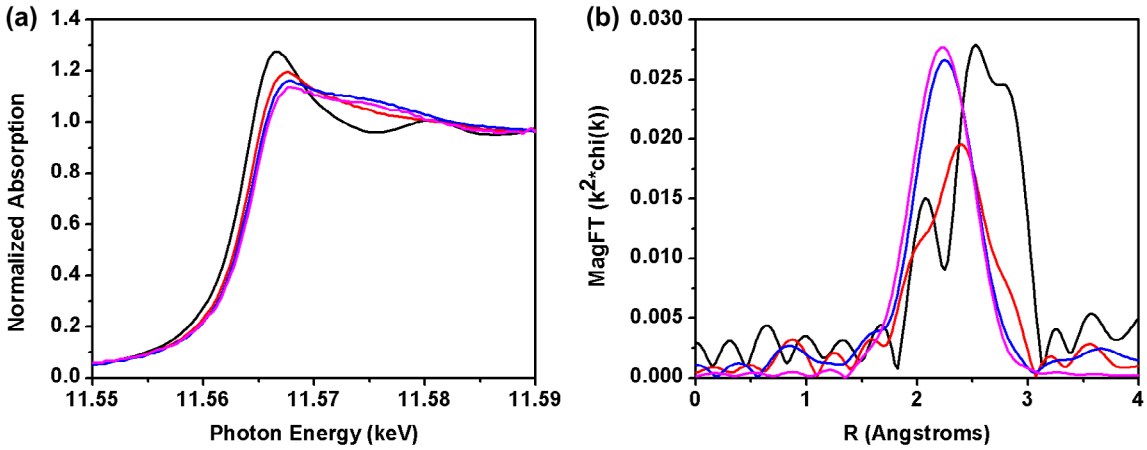

Figure 4. Pt L_{III} Edge (a) XANES spectra and (b) magnitude of the Fourier transform of the EXAFS of Pt (black), Cu–Pt(0.7) (red), Cu–Pt(2.3) (blue) and Cu–Pt(7.3) (magenta).

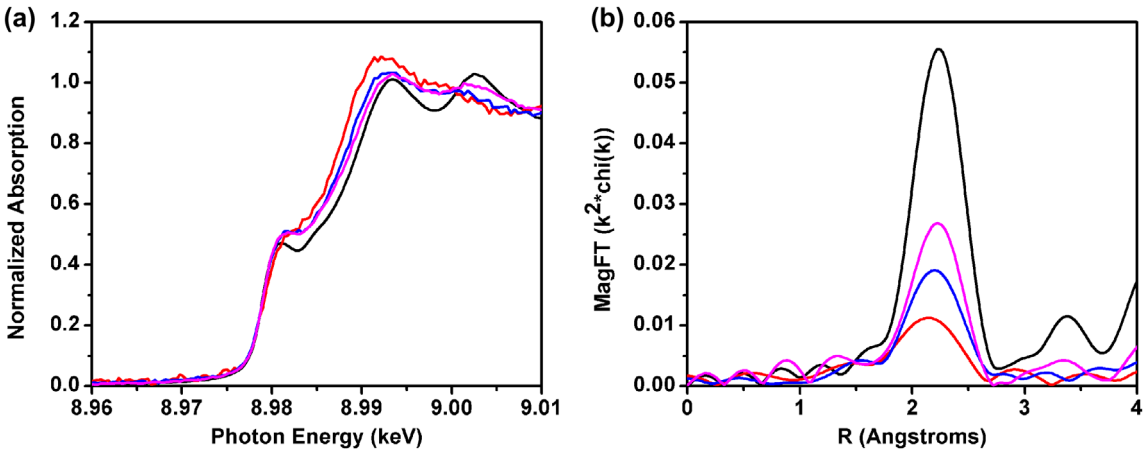

Figure 5. Cu K Edge (a) XANES spectra and (b) magnitude of the Fourier transform of the EXAFS of Cu foil (black), Cu–Pt(0.7) (red), Cu–Pt(2.3) (blue) and Cu–Pt(7.3) (magenta).

determined by the chemisorption, the resulting turnover rate (TOR) increased almost linearly for Pt–Cu catalysts with increasing Cu:Pt ratio (Figure 3(b)). Comparing with a TOR of 0.06 s^{-1} for Pt catalyst, the three Pt–Cu catalysts with increasing Cu:Pt ratio were measured with TORs of 0.17, 0.40, and 0.98 s^{-1} respectively, showing that introduction of Cu significantly promotes the TOR of Pt catalysts for propane dehydrogenation.

Table 3. EXAFS fitting parameters for Pt–Cu catalysts.

Catalyst	Edge	Edge energy (keV)	Scattering path	Coordination number	Bond distance (Å)	Debye Waller factor $\Delta\sigma^2$	Energy shift E_0
Pt	Pt L_{III}	11.5642	Pt–Pt	9.5	2.75	0.003	−1.0
Cu–Pt(0.7)	Pt L_{III}	11.5644	Pt–Pt	6.6	2.71	0.003	−2.2
			Pt–Cu	3.1	2.63	0.003	5.3
	Cu K		Cu–Pt	6.3	2.63	0.003	0.8
			Cu–Cu	2.9	2.55	0.003	−6.7
Cu–Pt(2.3)	Pt L_{III}	11.5646	Pt–Pt	3.4	2.71	0.003	−3.1
			Pt–Cu	7.3	2.58	0.003	4.0
	Cu K		Cu–Pt	2.7	2.58	0.003	0.6
			Cu–Cu	5.4	2.54	0.003	−2.9
Cu–Pt(7.3)	Pt L_{III}	11.5647	Pt–Cu	8.3	2.56	0.003	2.3
	Cu K		Cu–Cu	7.9	2.53	0.003	−1.7

In situ X-ray absorption spectroscopy

In situ X-ray absorption near-edge spectra (XANES) and Extended X-ray absorption fine structure (EXAFS) spectra were collected for the Pt and Pt–Cu catalysts at both the Pt L_{III} edge (11.564 keV) and Cu K edge (8.979 keV) to investigate the local structure around Pt and Cu atoms. The spectra were recorded at room temperature after the samples were pre-reduced in H_2/He at 550 °C for 30 min. The XANES spectra at both the Pt and Cu edges are shown in Figures 4(a) and 5(a) with corresponding edge energy reported in Table 3. At the Pt edge, all the spectra indicate metallic Pt as their white line intensity is slightly lower than that for Pt foil. While Pt foil has an edge energy of 11.5640 keV, the edge is slightly shifted to higher energy (11.5642 keV) for the monometallic Pt nanoparticle catalyst. Similar energy shift has been reported previously for Pt nanoparticle and corresponds to higher absolute energy of the lowest unoccupied level in the Pt 5d bands [24]. When Cu is introduced to the Pt catalyst, the edge energy further increases. For the three Pt–Cu catalysts with increasing Cu:Pt atomic ratio, the edge energy changes to 11.5644, 11.5646 and finally 11.5647 keV. This increase in edge energy along with a change in the shape of white line upon introduction of Cu in the catalysts suggest electronic interaction of Cu with metallic Pt atoms and formation of bimetallic nanoparticles. In the XANES spectra at Cu K edge shown in Figure 5(a), the intensity of the white line slightly increases and the shape of the XANES spectra change compared to that of the Cu foil. The change is most noticeable for Cu–Pt(0.7) and becomes less prominent for samples with lower Pt:Cu atomic ratio, indicating the change is induced by the Pt neighbors near the Cu atoms and Pt–Cu bimetallic nanoparticles are formed.

Figures 4(b) and 5(b) show the magnitude of the k^2 weighted Fourier Transform of the EXAFS spectra for the metal foil and all the Pt–Cu catalysts. In the spectra at Pt L_{III} edge, major differences could be found between the Pt catalysts and the Pt–Cu catalysts. The Pt catalyst show a three-peak pattern typical of Pt nanoparticles with a Pt–Pt bond distance of 2.75 Å and coordination number of 9.5 (Table 3). For Cu–Pt(0.7) which contains a relatively low amount of Cu in the catalyst, while the spectra still show a three-peak pattern, the peak position is shifted to lower R and the relative intensity of the three peaks changes, both indicating that the Pt–Pt scattering is strongly interfered by another scattering path, i.e. Pt–Cu. The interference is confirmed by the curve fitting, for which a satisfactory fit is only obtainable when both Pt–Pt and Pt–Cu scattering pairs are used. The fitting results in an average Pt–Pt distance at 2.71 Å and coordination number of 6.6 with an average Pt–Cu distance at 2.63 Å and coordination number of 3.1. The unusual low average Pt–Pt bond distance in Cu–Pt(0.7) compared to monometallic Pt likely implies that these Pt–Pt pairs are distorted because of the Cu neighbors which have a shorter bond distance. The two Pt–Cu catalysts with higher Cu:Pt atomic ratio give EXAFS with totally different shape. Only a single peak typical of Pt-3d metal scattering is observed. For Cu–Pt(2.3), both Pt–Pt scattering with an average coordination of 3.4 again at a bond distance of 2.71 Å and Pt–Cu scattering with an average coordination of 7.3 at a bond distance of 2.58 Å are found. The Pt–Cu coordination becomes dominant, which is expected as the atomic ratio of Cu:Pt increases. For Cu–Pt(7.3) sample, only a Pt–Cu scattering at 2.56 Å with a coordination number of 8.3 can be reliably fit suggesting that a Pt–Cu bimetallic structure is formed with few Pt–Pt neighbors.

At the Cu edge, a systematic change in the magnitude of the k^2 weighted Fourier Transform of the EXAFS spectra of the Pt–Cu catalysts with increasing Cu:Pt ratio are also seen. For the Cu–Pt(0.7) catalyst with relatively low Cu loading, the scattering peak intensity is very low, indicating a strong interference of Cu–Cu and Cu–Pt scattering. The fitted Cu–Pt bond distance 2.63 Å from this spectrum match the distance for Pt–Cu bond distance in the same sample and the Cu–Cu bond distance 2.55 Å is typical for metallic Cu. The Cu–Pt coordination number 6.3 is around 2 times that of the Pt–Cu coordination. Within the error of the EXAFS analysis these fit values are consistent with the Pt to Cu molar ratios. The relation between the ratio of coordination number and mole fraction of atoms in bimetallic particles ($MF_a \times CN_{ab} = MF_b \times CN_{ba}$ where M is the mole fraction

and CN_{ab}, for example is the coordination number of absorber atom A and scattering atom B) was proposed by Via and is also consistent with the fitting results for Cu–Pt(2.3) [25]. As more and more Cu is introduced to the sample, Cu–Cu scattering starts to dominate at the Cu edge, as can be seen from the increasing intensity of the EXAFS magnitude resulting from less Cu–Pt interference. For Cu–Pt(2.3) sample, an average bond distance of 2.58 Å with coordination number of 2.7 is fitted for Cu–Pt and corresponding value is 2.54 Å and 5.4 for Cu–Cu. The bond distance of Cu–Pt again agrees the fitting results for Pt–Cu at the Pt edge. For the Cu–Pt(7.3) with the highest Cu:Pt ratio, the EXAFS can be fitted with only Cu–Cu scattering at 2.53 Å and a coordination number of 7.9. While a low contribution from Cu–Pt scattering is expected, it is hard to determine a precise coordination number of this scattering path due to its very low intensity. Overall, the feature of the EXAFS at the Cu edge and the corresponding fitting results agree with the information from the Pt edge, both of which indicate formation of Pt–Cu bimetallic nanoparticles in these Pt–Cu catalysts. With increasing Cu:Pt atomic ratio, the average Cu coordination in both Pt and Cu EXAFSs increases.

In situ, synchrotron X-ray diffraction

The bimetallic Pt–Cu structure identified by XAS may be either an ordered intermetallic Pt–Cu compound, Pt–Cu solid solution where Pt in its fcc lattice is randomly substituted by Cu atoms, or a core shell nanoparticle with ordered or random surface structure. To investigate the structure of the Pt–Cu nanoparticles, *in situ* XRD was performed. For <3 nm small nanoparticles, synchrotron X-ray sources and *in situ* reduction was required for their structure to be resolved [26]. The XRD pattern was recorded after the catalysts were pre-reduced under H_2 at 550 °C and also after further cooled to room temperature in the same atmosphere. The patterns at room temperature showed the same feature as those obtained at 550 °C except for slight shifts in the peaks due to thermal disorder at high temperature. Therefore, the room temperature patterns are representative of the catalyst structure at reaction condition and are used to deduce structural information. The XRD patterns of the Pt and Pt–Cu catalysts are subtracted with the SiO_2 and instrumental background recorded at the same condition to isolate the diffraction from metals or alloys, and further normalized by per mol of metal atoms in the nanoparticle, which are shown in Figure 6 together with the corresponding simulated XRD pattern of the identified Pt–Cu phases. The simulation has taken into account a decrease in average bond distance by 0.02 Å typical for 2 nm nanoparticles due to strong surface contraction originated from high portion of coordination unsaturated surface atoms.

The XRD pattern for all the catalysts show features typical of nanoparticles with FCC crystal structure. All

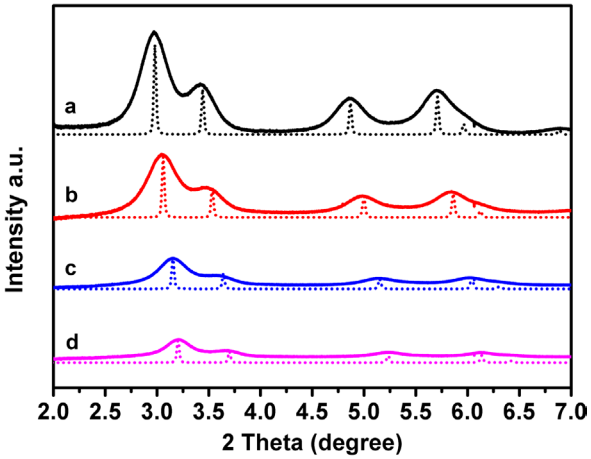

Figure 6. Background subtracted *in situ* XRD pattern of: (a) Pt (black, solid), (b) Cu–Pt(0.7) (red, solid), (c) Cu–Pt(2.3) (blue, solid) and (d) Cu–Pt(7.3) (magenta, solid) compared with the simulated XRD pattern of: (a) bulk FCC Pt (black, dotted), (b) Pt0.70Cu0.30 (red, dotted), (c) Pt0.32Cu0.68 (blue, dotted), and (d) Pt0.13Cu0.87 (magenta, dotted).

the diffraction peaks are strongly broadened compared to bulk materials, suggesting very small particle size. For each diffraction pattern, the first 3 main diffraction peaks correspond to the (1 1 1), (2 0 0), and (2 2 0) plane in the FCC structure and the forth peak results from two overlapping diffraction peaks from (3 1 1) and (4 0 0) reflections. The first and the third diffraction peak are not significantly overlapped by the neighboring peaks, therefore, their peak positions are used for Bragg's law analysis to obtain lattice constant and average bond distance of each sample, Table 4. Their peak FWHMs are used for Sherrer equation analysis to determine the crystallite size. Pt and Cu have the same FCC crystal type and form a solid solution over the whole composition range at high temperature. Therefore Vegard's law can be further applied to estimate the average composition of the bimetallic nanoparticles from the average bond distance of the Pt–Cu catalysts, Table 4.

For different samples with increasing Cu:Pt atomic ratio, the diffraction peaks shift to higher 2θ angles and the peak intensity decreases, both suggesting that more and more Cu is incorporated into the nanoparticles as shown by XAS previously. No superlattice diffraction is observed and the nanoparticle composition shown below is different from the ideal composition of ordered alloys, suggesting that Pt and Cu form solid solution structure. Since the same feature can be observed in both the patterns at 550 °C and the one at room temperature, this solid solution structure present at 550 °C and is maintained after fast cooling to room temperature. From the peak position of the (1 1 1) and (2 2 0) diffraction peaks, the lattice constant of the Pt nanocrystal in Pt catalyst is determined to be 3.92 Å. The value is smaller than the one for bulk Pt metal, which is expected for <3 nm Pt nanoparticles as its large portion of surface Pt atoms are coordination unsaturated, leading to lattice

Table 4. Results from *In situ* XRD data.

Catalyst	Lattice constant (Å)	Bond distance (Å)	Pt composition (%)	Particle size (nm)
Pt	3.92	2.77	100	2.2
Cu–Pt(0.7)	3.82	2.70	70	2.0
Cu–Pt(2.3)	3.70	2.61	32	2.0
Cu–Pt(7.3)	3.63	2.57	13	2.3

contraction [27]. The corresponding Pt–Pt bond distance is 2.77 Å and the crystallite size is found to be 2.2 nm for this sample, slightly smaller than the average particle size determined from the STEM image (2.5 nm) due to the error in both techniques and likely also extra diffraction peaks broadening coming from lattice strain induced by surface contraction. For Cu–Pt(0.7) catalyst, the lattice constant decreases to 3.82 Å, giving an average bond distance of 2.70 Å. According to Vegard's law, this bond distance corresponds to a Pt–Cu solid solution with 70% Pt based on a standard bond distance of 2.77 Å for Pt and 2.54 Å for Cu obtained under the same experimental condition for nanoparticles in similar size. The solid solution crystallite is in a size of 2.0 nm, similar to the Pt catalyst and also the size determined from STEM. The same analysis on Cu–Pt(2.3) catalyst results in an average metal-metal bond distance of 2.61 Å and Pt concentration of 32%, which confirms that more Cu is incorporated into the bimetallic nanoparticles for this sample. Although the nanoparticle composition is now Cu-rich rather than Pt rich, its crystallite size remains 2.0 nm. With an even higher Cu:Pt ratio, for the Cu–Pt(7.3) catalyst, its diffraction peak is further shifted to higher angle that is very close to Cu nanoparticles. Corresponding lattice constant is 3.63 Å. The average metal-metal bond distance is 2.57 Å and Vegard's law gives a Pt concentration of 13% (Table 4).

Discussion

Structure analysis of Pt–Cu catalysts

The structure of Pt–Cu catalysts with different Cu:Pt ratios have been investigated by *in situ* X-ray diffraction and X-ray absorption spectroscopy. XRD reveals the crystal structure of the Pt–Cu nanoparticles, showing that all the Pt–Cu catalysts form solid solution in which Pt and Cu randomly distribute throughout the fcc lattice. As the atomic ratio of Cu: Pt increases from 0.7 to 2.3 and eventually 7.3, more Cu is incorporated into the bimetallic nanoparticles and the composition of the Pt–Cu nanoparticles changes from 30% Cu to 68% Cu and finally 87% Cu. The nanoparticle composition obtained is very close to the expected value from the nominal loading, suggesting that all the Pt and Cu are reduced, which has also been shown by the metallic white line feature in the XANES. The increasing Cu content in this series of Pt–Cu nanoparticle catalysts are confirmed by XAS, as shown by increasing shift in Pt edge energy from 0.4 to 0.7 eV and Pt–Cu coordination from around 3.1–8.3. This change in the solid solution composition also results in decreased lattice constant and corresponding average metal-metal bond distance. As reflected by XRD, the Pt–Pt bond distance for Pt catalyst was measured to be 2.77 Å. With increasing Cu loading, the average bond distance significantly decrease to 2.70, 2.61 Å and eventually 2.57 Å. The change corresponds to increasing coordination number of Pt–Cu bond and Cu–Cu bond as shown by EXAFS fitting. The fitted Pt–Cu bond distance for the three Pt–Cu catalysts also decreases from 2.63 to 2.58 Å and further 2.56 Å, indicating these bonds of Pt–Cu neighbor pairs are increasingly distorted to shorter length as surrounded by more and more smaller Cu atoms and less Pt atoms.

The particle size of the Pt and Pt–Cu catalysts is determined from XRD and STEM to be between 2 and 3 nm. For the three Pt–Cu catalysts, the particle size does not change significantly compared with the monometallic Pt catalysts. Assuming a totally random distribution of Pt and Cu atoms, the dispersion of the Pt–Cu catalysts should also be similar to the monometallic Pt. The measured dispersion of the Pt–Cu catalysts, however, is lower than that of the monometallic Pt catalysts, which suggests that a minor enrichment of Cu on the catalyst surface that does not chemisorb CO at room temperature may be possible. Bimetallic nanoparticle with solid solution structure including Pt–Cu has been known to suffer from surface segregation [28].

The promotional effect of copper

Among monometallic nanoparticle catalysts, Pt has the highest alkane dehydrogenation selectivity compared to the other group VIII metals (Pd, Ir, Rh etc.). The Pt catalyst exhibits a propylene selectivity of 61% at 20% propane conversion. When Cu is introduced to the catalyst, for the Cu–Pt(0.7) catalyst with relatively low Cu content (30%), the selectivity is slightly improved to 72%. High selectivity, however, is achieved only when higher level of Cu are introduced. For Cu–Pt(2.3) and Cu–Pt(7.3) with Cu composition of 68 and 87%, their dehydrogenation selectivity increase to 90 and 96%, respectively. The propylene selectivity increases almost linearly with the increase in the level of the Cu in the solid solution before it reaches a very high value close to 100% (Figure 7). In the Cu–Pt(0.7), Pt-rich solid solution is formed, which means there is still sufficient Pt–Pt neighbors on the nanoparticles surface. Correspondingly, there is significant activity for hydrogenolysis and the catalyst dehydrogenation selectivity is poor. The Cu–Pt(7.3) catalyst with 87% Cu, instead, forms very Cu-rich solid solution. In this structure, only Pt–Cu but no Pt–Pt neighbors are identified in EXAFS, suggesting Pt atoms are isolated from the other Pt atoms by inactive or much less active Cu atoms. In this structure, there are enough Cu atoms, although distributed randomly, surrounding the catalytic Pt sites.

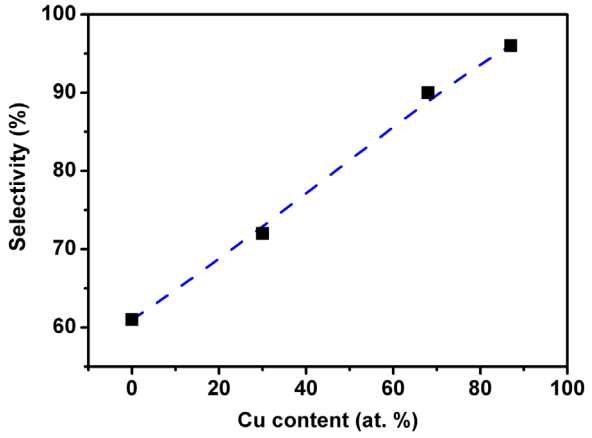

Figure 7. Dehydrogenation Selectivity vs. Cu content in atomic percentage.

As a result, almost no Pt ensembles remain, which suppresses hydrogenolysis side reactions and contributes to the very high propylene selectivity of this catalyst for propane dehydrogenation reaction. Like intermetallic alloy nano-particle catalysts, a bimetallic catalyst with solid solution structure can also be highly selective to propane dehydrogenation given sufficient amount promoter atoms are incorporated.

To improve the Pt–Cu catalyst selectivity to above 90%, it seems that higher than about 70% of Cu is needed in the bimetallic nanoparticles. However, previously it was reported that for a Pd-In catalyst, less than 20% of promoter is needed for the catalyst to become highly selective (>95%) to ethane dehydrogenation.

Similarly, for Pd–Zn propane dehydrogenation catalysts small amounts of surface Zn present as an alloy were required for high selectivity (although the content of Zn needed was not determined) [12–14]. This very different effect in catalytic performance upon introduction of different amount of promoter atoms very likely originates from formation of different bimetallic structures. Introduction of In or Zn results not only in formation of ordered PdIn or PdZn alloys, but also that the alloys preferentially form on the catalyst surface. Both effect leads to efficient isolation of surface Pd sites with only small amount of promoter atoms. When Cu is added, Pt and Cu form solid solution in which Cu is randomly distributed throughout the nanoparticle instead of preferably on the surface. As a result, a large amount of Cu is needed for isolation of surface Pt atoms. This difference in the catalyst performance with change in promoter metal loading can be used to distinguish between formation of an ordered surface alloy, or a solid solution structure, i.e. alloy selectivity improve with small amounts of promoter and no further increase are obtained with increasing promoter content, while in solid solution the dehydrogenation selectivity increases with the promoter level and higher promoter to Pt levels are required for high selectivity.

Increasing the atomic ratio of Cu:Pt not only results in increased dehydrogenation selectivity, but also continuous improvement of catalytic rate per gram Pt and TOR. From Cu:Pt ratio of 0, to 0.7, to 2.3, to 7.3, the catalytic rate per gram Pt increase by 2 and 3-fold with each increase in Cu:Pt ratio. Comparing the Cu–Pt(7.3) with the monometallic Pt catalyst, the rate increases by almost 14 times in total, from 8.8×10^{-5} mol g^{-1} s^{-1} to 1.2×10^{-3} mol g^{-1} s^{-1}. This means that using Pt–Cu catalysts with a high Cu:Pt ratio, certain propane dehydrogenation conversion could be achieved with less Pt compared to monometallic Pt catalyst. The TOR per mole of surface Pt of Pt–Cu catalysts also significantly increases compared to monometallic Pt. For the TOR estimated from the dispersion obtained by CO chemisorption, the increase is greater for catalysts with higher Cu:Pt atomic ratio (Figure 7). A TOR of 0.98 s^{-1} of Cu–Pt(7.3) catalyst is 16 times higher than the TOR of 0.06 s^{-1} for monometallic Pt and also higher than the typical TOR values (0.1–0.5 s^{-1}) of Pt-Sn catalysts under similar reaction condition [1].

The Pt L_{III} XANES spectra show an increase in the edge energy and decrease in the white line intensity of Pt–Cu compared to Pt consistent with a change in the electronic properties of the Pt 5d orbitals in the bimetallic nanoparticles. The increase in XANES energy indicates an upward shift in the unfilled valance states of Pt while the decrease in the white line intensity suggests higher occupancy of the 5d orbitals. A shift to higher energy in the Pt–Cu XANES spectra suggests that the energy of the empty 5d orbitals are at higher energy compared to Pt. This also suggests that the filled 5d orbitals in Pt–Cu are lower energy than those in monometallic Pt due to Pt–Cu bond formation. A shift to lower energy would result in less hybridization of the 5d with the 6s and 6p orbitals leading to slightly higher electron density in the 5d states and a decrease in the white line intensity. A decrease in the energy of the 5d states in Pt–Cu bimetallic catalysts may also lead to a decrease in the energy of adsorption of reactants and products and increase in the TOR.

Conclusion

Monometallic Pt and three Pt–Cu catalysts with similar particle size between 2 and 3 nm and different atomic ratios of Cu:Pt have been synthesized, characterized and tested for propane dehydrogenation. Introduction of Cu increased the dehydrogenation selectivity and TOR by forming solid solution with Pt. For the series of Pt–Cu catalysts, the propylene selectivity increased almost linearly with increasing Cu level in the solid solution. At low Cu loading for Cu–Pt(0.7) catalyst, Pt-rich solid solution was formed and the catalyst selectivity slightly increased. Pt–Cu catalysts with high Cu loading formed Cu-rich solid solution, and became more Cu-rich with increasing the loading of Cu. In Cu–Pt(7.3) catalyst, the

Pt–Cu solid solution contained 87% Cu and the active Pt atoms were almost all isolated by non-catalytic Cu atoms. This geometric effect contributed to the high propylene selectivity (96%) of this catalyst. The continuous improvement of catalyst selectivity in response to increasing content of promoter in the nanoparticle was different from a sharp increase of selectivity upon introduction of very low amount of promoter atoms previously seen for Pt promoted by Sn/Ga/Zn/In, and was due to formation of solid solution structure with random atomic distribution instead of surface intermetallic alloy in which the promoter atoms form ordered structure with noble metal preferably on the catalyst surface. For Pt–Cu catalyst, high selectivity is only obtained when the Cu level in the nanoparticle is high enough, which can be used as a sign to differentiate formation of solid solution from ordered alloy structure. The dehydrogenation reaction rate per gram Pt and TOR of the Pt–Cu catalysts are also significantly improved by promoter Cu. It seems that the TOR increases linearly with Cu:Pt atomic ratio. For the Cu–Pt(7.3) catalyst with relatively high Cu:Pt ratio, the rate per gram and TOR are around 16 times higher than that of monometallic Pt.

Acknowledgements

The authors also acknowledge the use of beamline 11-ID-C. We thank Evan Wegener for experimental assistance on XAS and CO chemisorption analysis, and Arthur Shih for experimental assistance on AAS analysis. Use of the Advanced Photon Source was supported by the U.S. Department of Energy, Office of Basic Energy Sciences [grant number DE-AC02-06CH11357]. MRCAT operations, beamline 10-BM, are supported by the Department of Energy and the MRCAT member institutions.

Disclosure statement

No potential conflict of interest was reported by the authors.

Funding

This work was supported by the School of Chemical Engineering, Purdue University.

References

[1] Sattler JJ, Ruiz-Martinez J, Santillan-Jimenez E, et al. Catalytic dehydrogenation of light alkanes on metals and metal oxides. Chem Rev. 2014;114:10613–10653.
[2] Siddiqi G, Sun P, Galvita V, et al. Catalyst performance of novel Pt/Mg(Ga)(Al)O catalysts for alkane dehydrogenation. J Catal. 2010;274:200–206.
[3] Passos FB, Aranda DA, Schmal M. Characterization and catalytic activity of bimetallic Pt-In/$Al_2O_3$and Pt-Sn/Al_2O_3 catalysts. J Catal. 1998;178:478–488.
[4] Virnovskaia A, Morandi S, Rytter E, et al. Characterization of Pt, Sn/Mg(Al)O catalysts for light alkane dehydrogenation by FT-IR spectroscopy and catalytic measurements. J Phys Chem C. 2007;111:14732–14742.
[5] Jablonski E, Castro A, Scelza O, et al. Effect of Ga addition to Pt/Al_2O_3 on the activity, selectivity and deactivation in the propane dehydrogenation. Appl Catal A Gen. 1999;183:189–198.
[6] Galvita V, Siddiqi G, Sun P, et al. Ethane dehydrogenation on Pt/Mg(Al)O and PtSn/Mg(Al)O catalysts. J Catal. 2010;271:209–219.
[7] Shen J, Hill JM, Watwe RM, et al. Microcalorimetric, infrared spectroscopic, and DFT studies of ethylene adsorption on Pt/SiO_2 and Pt–Sn/SiO_2 catalysts. J Phys Chem B. 1999;103:3923–3934.
[8] Silvestre-Albero J, Sanchez-Castillo MA, He R, et al. Microcalorimetric, reaction kinetics and DFT studies of Pt–Zn/X-zeolite for isobutane dehydrogenation. Catal Lett. 2001;74:17–25.
[9] Sun P, Siddiqi G, Vining WC, et al. Novel Pt/Mg(In)(Al)O catalysts for ethane and propane dehydrogenation. J Catal. 2011;282:165–174.
[10] Sun P, Siddiqi G, Chi M, et al. Synthesis and characterization of a new catalyst Pt/Mg(Ga)(Al)O for alkane dehydrogenation. J Catal. 2010;274:192–199.
[11] Vu BK, Song MB, Ahn IY, et al. Pt–Sn alloy phases and coke mobility over Pt–Sn/Al_2O_3 and Pt–Sn/$ZnAl_2O_4$ catalysts for propane dehydrogenation. Appl Catal A Gen. 2011;400:25–33.
[12] Childers DJ, Schweitzer NM, Shahari SMK, et al. Modifying structure-sensitive reactions by addition of Zn to Pd. J Catal. 2014;318:75–84.
[13] Wu Z, Wegener EC, Tseng H-T, et al. Pd–In intermetallic alloy nanoparticles: highly selective ethane dehydrogenation catalysts. Catal Sci Technol. 2016;6:6965–6976.
[14] Gallagher JR, Childers DJ, Zhao H, et al. Structural evolution of an intermetallic Pd–Zn catalyst selective for propane dehydrogenation. Phys Chem Chem Phys. 2015;17:28144–28153.
[15] Okamoto H. Phase diagram for binary alloys. Vol. 828. Materials Park (OH): ASM International Member/Customer Service Center; 2000.
[16] Hamid SBD-A, Lambert D, Derouane EG. Dehydroisomerisation of n-butane over (Pt, Cu)/H-TON catalysts. Catal Today. 2000;63:237–247.
[17] Veldurthi S, Shin C-H, Joo O-S, et al. Promotional effects of Cu on Pt/Al_2O_3 and Pd/Al_2O_3 catalysts during n-butane dehydrogenation. Catal Today. 2012;185:88–93.
[18] Han Z, Li S, Jiang F, et al. Propane dehydrogenation over Pt–Cu bimetallic catalysts: the nature of coke deposition and the role of copper. Nanoscale. 2014;6:10000–10008.
[19] Komatsu T, Tamura A. Pt_3Co and PtCu intermetallic compounds: promising catalysts for preferential oxidation of CO in excess hydrogen. J Catal. 2008;258:306–314.
[20] Schneider CA, Rasband WS, Eliceiri KW. NIH image to imageJ: 25 years of image analysis. Nat Methods. 2012;9:671–675.
[21] Ressler T. WinXAS: a program for X-ray absorption spectroscopy data analysis under MS-Windows. J Synchr Radiat. 1998;5:118–122.
[22] Toby BH, Von Dreele RB. GSAS-II: the genesis of a modern open-source all purpose crystallography software package. J Appl Crystallogr. 2013;46:544–549.
[23] Lutterotti L, Matthies S, Wenk H. MAUD: a friendly Java program for material analysis using diffraction. IUCr Newsletter of the CPD. 1999;21:14–15.
[24] Lei Y, Jelic J, Nitsche LC, et al. Effect of particle size and adsorbates on the L3, L2 and L1 X-ray absorption near edge structure of supported Pt nanoparticles. Top Catal. 2011;54:334–348.

[25] Via G, Drake K Jr, Meitzner G, et al. Analysis of EXAFS data on bimetallic clusters. Catal Lett. 1990;5: 25–33.
[26] Gallagher JR, Li T, Zhao H, et al. In situ diffraction of highly dispersed supported platinum nanoparticles. Catal Sci Technol. 2014;4:3053–3063.
[27] Lei Y, Zhao H, Rivas RD, et al. Adsorbate-induced structural changes in 1–3 nm platinum nanoparticles. J Am Chem Soc. 2014;136:9320–9326.
[28] Yu W, Porosoff MD, Chen JG. Review of Pt-based bimetallic catalysis: from model surfaces to supported catalysts. Chem Rev. 2012;112:5780–5817.